Original Article

Delivery of Wnt inhibitor WIF1 via engineered polymeric microspheres promotes nerve regeneration after sciatic nerve crush

Journal of Tissue Engineering
Volume 13: 1–14

DOI: 10.1177/20417314221087417
journals.sagepub.com/home/tej
SAGE

Na Zhang[1], Junquan Lin[1], Jiah Shin Chin[1,2], Christian Wiraja[1], Chenjie Xu[1,3], Duncan Angus McGrouther[4] and Sing Yian Chew[1,5,6]

Abstract

Injuries within the peripheral nervous system (PNS) lead to sensory and motor deficits, as well as neuropathic pain, which strongly impair the life quality of patients. Although most current PNS injury treatment approaches focus on using growth factors/small molecules to stimulate the regrowth of the injured nerves, these methods neglect another important factor that strongly hinders axon regeneration—the presence of axonal inhibitory molecules. Therefore, this work sought to explore the potential of pathway inhibition in promoting sciatic nerve regeneration. Additionally, the therapeutic window for using pathway inhibitors was uncovered so as to achieve the desired regeneration outcomes. Specifically, we explored the role of Wnt signaling inhibition on PNS regeneration by delivering Wnt inhibitors, sFRP2 and WIF1, after sciatic nerve transection and sciatic nerve crush injuries. Our results demonstrate that WIF1 promoted nerve regeneration ($p < 0.05$) after sciatic nerve crush injury. More importantly, we revealed the therapeutic window for the treatment of Wnt inhibitors, which is 1 week post sciatic nerve crush when the non-canonical receptor tyrosine kinase (Ryk) is significantly upregulated.

Keywords

Peripheral nerve injury, nerve guidance conduits, Wnt signaling inhibitors, electrospinning, neural tissue engineering

Date received: 24 November 2021; accepted: 27 February 2022

Introduction

Many pathways are dysregulated after sciatic nerve injuries[1,2] and the dysregulation of certain pathways may lead to nerve growth inhibition,[3,4] among which the Wnt signaling pathway is one of the most common pathways.[5,6] However, studies on PNS repair have paid minimal attention to explore the roles of pathway inhibition on nerve regeneration. Hence, in this work, instead of using growth factors to promote the regeneration of injured sciatic nerves, we focused on modulating Wnt signaling. In addition, we explored the potential time points at which the inhibition of this pathway would provide the most effective treatment outcomes, a consideration that is important but often neglected.

Wnt signaling pathways are essential during early and late nervous system development. These pathways modulate axon branching, axon outgrowth, as well as growth

[1]School of Chemical and Biomedical Engineering, Nanyang Technological University, Singapore, Singapore
[2]NTU Institute for Health Technologies, Interdisciplinary Graduate School, Nanyang Technological University, Singapore, Singapore
[3]Department of Biomedical Engineering, City University of Hong Kong, Kowloon, China
[4]Department of Hand and Reconstructive Microsurgery, Singapore General Hospital, Singapore, Singapore
[5]Lee Kong Chian School of Medicine, Nanyang Technological University, Singapore, Singapore
[6]School of Materials Science and Engineering, Nanyang Technological University, Singapore, Singapore

Corresponding author:
Sing Yian Chew, School of Chemical and Biomedical Engineering, Nanyang Technological University, 62 Nanyang Drive, N1.2-B2-20, Singapore 637459, Singapore.
Email: sychew@ntu.edu.sg

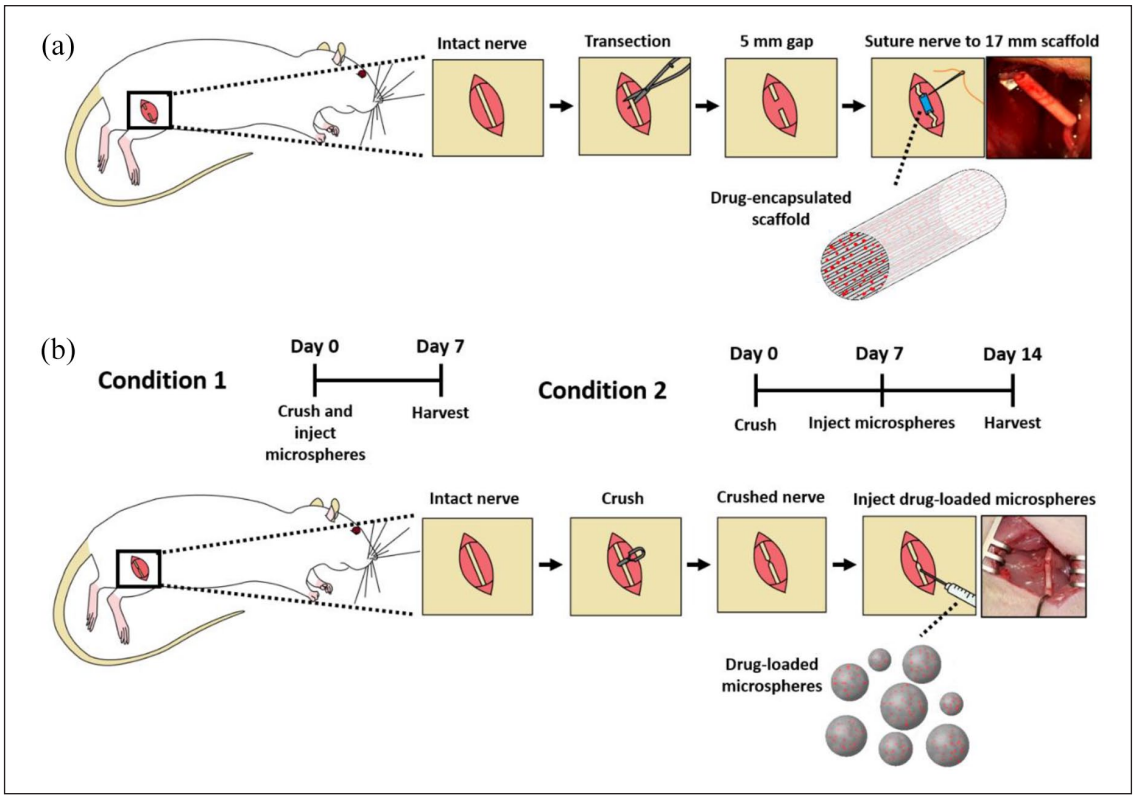

Figure 1. Schematic diagrams. (a) Illustration of the procedures of sciatic nerve transection and nerve guidance conduit implantation. (b) Two conditions of experimental settings. Condition 1 is that the rats underwent sciatic nerve crush and received immediate treatment. Condition 2 is that the rats received a delayed treatment for 7 days from sciatic nerve crush. Schematic diagram of sciatic nerve crush and the administration of drug loaded PLGA microspheres.

cone and synapse formation.[7] The exact biological effects of Wnt ligands, however, is complex and largely dependent on the Wnt receptors to which these ligands bind. For instance, Wnt ligands that activate the canonical Wnt signaling generally promote axonal growth,[8,9] whereas Wnt ligands that activate the non-canonical Wnt-Ryk pathways inhibit axonal growth.[3,4,10,11] Correspondingly, the presence of repulsive non-canonical Wnt ligands contributed to axon growth inhibition and nerve retraction within the injured central nervous system (CNS). Conversely, blocking the non-canonical Wnt signaling promoted axonal growth and functional recovery.[6,12]

Although the above findings reveal that the activation of Wnt-Ryk signaling pathway leads to nerve retraction in the CNS, the roles of Wnt-Ryk signaling and whether the addition of Wnt inhibitors could promote nerve regeneration in the PNS remains unknown. Here, we hypothesize that the activation of the repulsive Wnt signaling (i.e. Wnt-Ryk signaling) could result in the inhibition of nerve regeneration after sciatic nerve injury. Hence, by inhibiting the repulsive Wnt signaling using Wnt signaling inhibitors, nerve regeneration after sciatic nerve injury could be promoted.

Specifically, we incorporated two Wnt inhibitors (i.e. sFRP2 and WIF1) and investigated their effects on nerve regeneration after sciatic nerve injuries. In order to overcome the short lifespan of such protein-based therapeutics, biomaterials-based delivery platforms (e.g. electrospun fibers[13–19] and polymeric microspheres[20–22]) were utilized for controlled delivery so as to prolong the availability of these proteins. Due to the drastic difference in signaling pathway changes between sciatic nerve transection versus crush injury,[23–25] as well as the severity of the injuries, the two delivery platforms were analyzed in this study to investigate how Wnt signaling inhibition affects nerve regeneration outcomes. In the case of nerve transection injuries, these two Wnt inhibitors were encapsulated within nerve guidance conduits that consisted of aligned electrospun fibers. On the other hand, to treat crushed sciatic nerves, the two Wnt inhibitors were encapsulated into polylactic-co-glycolic acid (PLGA) microspheres that were injected distally to the injury sites (Figure 1).

Materials and methods

Materials

Polycaprolactone (PCL, molecular weight 45–80 kDa), 2,2,2-trifluoroethanol (TFE, ⩾99.0%), (Poly(ethylene glycol), PEG, Mn 400), Poly(D,L-lactide-co-glycolide) lactide: glycolide (50:50), PLGA, molecular weight 30k–60k, Span® 80 (S6760), Poly(vinyl alcohol) (PVA, molecular

weight 9k–10k), poly-D-Lysine (PDL) (P0899), and Bovine serum albumin (BSA ~66 kDa molecular weight) were purchased from Sigma-Aldrich, USA. Alexa-Fluor 488 goat anti-Chicken, Alexa-Fluor 555 goat anti-Rabbit, 555 goat anti-Mouse, DAPI (4′,6-diamidino-2-phenylindole), paraformaldehyde (PFA, 7,230,681), 10× phosphate buffered saline (PBS; pH = 7.4), goat serum, laminin (23,017,015), neurobasal medium, B-27 supplement, Glutamax supplement, Fluoromount-G™ (00-4958-02), and Pierce™ BCA Protein Assay Kit (23,225) were obtained from Life Technologies, USA. Mouse anti-βIII Tubulin (Tuj1) (801,202) and Chicken anti-Neurofilament 200 (NF200) (822,601) were purchased from Biolegend. Recombinant Human WIF-1 Protein (1341-WF) and Recombinant Human sFRP2 Protein (6838-FR) were obtained from R&D System. Nerve growth factor (NGF) was purchased from PeproTech. Fetal Bovine Serum (FBS) was acquired from Research Instruments.

Methods

In vitro scaffold fabrication for the culture of dorsal root ganglion explants. The fabrication of the in vitro aligned fiber scaffolds were carried out following our published protocols.[14,26] Briefly, 50 mg of PCL (molecular weight 45 kDa) was melted at 60°C before being cooled down to room temperature. The resulting block of PCL polymer was then cut into pieces of 2 cm × 1 cm × 0.5 cm before they were sectioned into 20 µm thin strips using a cryostat (Lecia CM1950) (Final dimension: 1 cm × 0.5 cm × 0.002 cm). Thereafter, the sterilized 20 µm PCL sheets were placed on glass coverslips (diameter: 18 mm) and heated at 50°C to generate a 1 cm × 1 cm cell seeding area before six of these coverslips were placed on the rotating wheel for the collection of electrospun fibers. A lower molecular weight PCL (45 kDa) was used instead of the 80 kDa PCL because the former melts faster and is easier to section into thin slices with the cryostat.

For electrospinning, the homogenous solution (80 kDa PCL, 14 wt%) was loaded into a syringe connected with a 21-gauge needle and dispensed at a fixed rate of 1.0 mL/h using a syringe pump. Positive 4 kV and negative 4 kV were then applied to the polymer solution and the rotating collector, respectively. The syringe and the collector (speed: 2400 rpm) were separated at 11 cm apart. Electrospun fibers were then collected and secured on the coverslips using inert silicone glue to prevent the fibers from detaching.

The morphology of the aligned fiber substrates was evaluated by scanning electron microscopy (SEM) (JEOL, JSM-6390LA, Japan) under an accelerating voltage of 10 kV after sputter-coating with platinum for 100 s at 10 mA. The average fiber diameters and alignment of the fibers were then quantified by measuring 50 fibers from high magnification images (2500x) using Image J software (NIH, USA, Supplemental Figure S1).

In vitro culture of dissociated DRG neurons and DRG explants. The isolation of DRG neurons from rat pups was approved by the Institutional Animal Care and Use Committee (IACUC) at Nanyang Technological University (Protocol number: A333). Dissociated DRG neurons were obtained from pups (postnatal day 2–3). The DRGs were harvested and the membrane was removed to minimize the contamination of other cells before they were digested with 1 mL of collagenase (10 mg/mL) at 37°C for 90 min, followed by 0.25% trypsin at 37°C for 15 min. After being homogenized, the cell suspension was passed through a 70 µm cell strainer (BD, Bioscience, USA) and the cells were seeded onto PDL (100 µg/mL) and laminin (10 µg/mL) coated 24-well plates at a density of 15,000 cells per well. Cultures were maintained in Neurobasal media containing 50 ng/mL of NGF, 10% FBS, 2% B-27 Supplement, Penicillin-Streptomycin (10 µg/mL), and 1% GlutaMAX. To test the effects of sFRP2 and WIF1 and identify the optimal drug concentrations for neurite outgrowth, serial dilution was performed. Specifically, the drugs were firstly reconstituted at 500 µg/mL in sterile, 1 × PBS containing 0.1% BSA as per recommended. The drugs were then further diluted in the culture medium and the final concentrations were set as follows: 10, 25, 50, 75, 100 ng/mL of sFRP2 or WIF1. The concentrations of sFRP2 and WIF1 tested here are based on the literature where similar concentrations were evaluated on dopaminergic neuron[27] and other cells,[28] respectively. The drugs were administrated 1 day after cell seeding. The cells were fixed with 4% PFA for 20 min 2 days after the treatment.

On the other hand, the culture of DRG explants were referred from our previous work.[26] Briefly, the DRGs were harvested and the membranes on the DRGs were removed. Thereafter, the DRGs were washed once with 1 × PBS and seeded directly on PDL and laminin coated aligned fiber scaffolds. Detachment of the DRG explants was prevented by adding in the culture medium gently. One day after seeding, the DRG explants were treated with 10, 50, 100, 200, 250, 500 ng/mL and 1 µg/mL of sFRP2 or WIF1. The DRGs were then fixed with 4% PFA for 20 min 2 days after the treatment.

Fabrication and characterizations of nerve guidance conduits

PCL film. The fabrication of drug loaded nerve guidance conduit was referred from our previous work.[26] Briefly, 70 mg of PCL pellets (molecular weight 45 kDa) were placed in between two pieces of metal sheets (15 cm × 25 cm) and pressed into a 50 µm thin PCL film using a heat press machine (Carver, Model 4128) at 80°C and 0.2 GPa. The resulting PCL film was cut into strips (i.e. 34 cm in length and 1 cm in width) before they were fixed around a rotating collector.

Preparation of PCL-PEG solution for the fabrication of nerve guidance conduit. The PCL-PEG solution was

prepared and the volume ratio of PCL to PEG was 8:2. Briefly, PCL (molecular weight 80 kDa) was dissolved in TFE to obtain a 14 wt% solution. Thereafter, PEG (i.e. 30 wt%) was dissolved in PBS and loaded with either 40 μg of sFRP2 or 40 μg of WIF1 containing 0.1% BSA. The homogenous solution (i.e. PCL and PEG) was then loaded into a syringe connected with a 21-gauge needle and dispensed at a fixed rate of 1.0 mL/h using a syringe pump. Positive 8 kV and negative 4 kV were then applied to the tip of the syringe and the rotating collector, respectively. The syringe and the collector were separated at 11 cm apart. The electrospun fibers were then collected on the PCL strip, which was fixed around a rotating collector (speed: 1200 rpm) during the electrospinning process. Thereafter, the PCL strip with aligned fibers was cut into small strips that were 17 mm in length before they were rolled into a conduit using a glass capillary with an outer diameter of 2 mm. This 34 cm PCL strip can be used to make twenty 17 mm nerve conduits and the theatrical loading of drug was 2 μg each. Based on our own experience in spinal cord injury treatment, 2 μg of miR therapeutics is sufficient to achieve a biological effect such as enhanced myelination after spinal cord hemi-incision injury[14] or enhanced axon regeneration after spinal cord transection injury.[13] Lastly, the edge of the conduit was sealed with 14 wt% PCL polymer solution. The nerve guidance conduits were then stored at −20°C for future usage.

The blank and drug-loaded nerve guidance conduits were cut in liquid nitrogen so as to preserve their cross-sectional structures. Part of the nerve conduit was cut open to expose the inner fiber surface. Both the cross-sectioned nerve guidance conduits along with their corresponding inner fiber surface were viewed under SEM. For inner fibers, 10 regions-of-interest (ROIs) were imaged and the average fiber diameter and fiber alignment were obtained by quantifying 50 individual fibers using ImageJ software (NIH, USA).

Sciatic nerve transection and nerve guidance conduit implantation. All the animal experiments were approved by the Institutional Animal Care and Use Committee (IACUC) at Nanyang Technological University (Protocol number: A0334). Female Sprague-Dawley rats (12 weeks, 250–300 g) were obtained from In Vivos Pte Ltd (Singapore) and divided into three groups, receiving either blank nerve conduits ($n=4$), sFRP2 ($n=4$), or WIF1 ($n=4$) encapsulated nerve guidance conduits. The schematic diagram of the surgical procedures is shown in Figure 1(a) and the experimental descriptions can be found in Supplemental Table S1a. Briefly, rats were anesthetized with an intraperitoneal injection of ketamine (73 mg/kg) and xylazine (7.3 mg/kg). All animals were injected with buprenorphine subcutaneously (0.05 mg/kg) before surgery. The surgical field was shaved and cleaned with 70% ethanol and treated with betadine. Under the surgery microscope, the right sciatic nerve was exposed through a posterior thigh muscle-splitting incision and 5 mm of the nerve was resected. A 17 mm nerve conduit was then sutured to the proximal stump and distal stump for about 1 mm respectively using a 11–0 nylon monofilament (Ethicon Inc) suture so as to bridge a 15 mm nerve lesion gap. The nerve guidance conduit was placed in parallel with the main trunk of the sciatic nerve. All nerve conduits were filled with 10 μL of PBS prior to implantation. Lastly, the muscles and skin were closed.

Fabrication and characterizations of drug loaded PLGA microspheres. The drug loaded PLGA microspheres were fabricated using double emulsion method. Briefly, 10 mg of PLGA powder was dissolved in chloroform containing 1% of Span80 (v/v). Next, 50 μg of sFRP2 or WIF was dissolved in 25 μL of 1 × PBS containing 0.1% BSA and added into the PLGA solution and homogenized using a homogenizer. Following that, the homogenized emulsion was added into 2% PVA solution and homogenized again. The resulting emulsion was covered with a piece of parafilm and stirred on a headplate at 37°C for 4 h to evaporate the organic solvent. The leftover emulsion was spun down and washed with washing buffer (i.e. 1 × PBS) for three times before they were lyophilized for future usage. A model protein, BSA was loaded into PLGA microspheres to mimic the drugs for characterization purposes using the same fabrication protocol. The washing buffer was kept so as to measure the amount of BSA inside. Firstly, the morphology of PLGA microspheres was obtained under scanning electron microscopy (SEM). The size of the particle was calculated by measuring 100 individual microspheres using Image J software.

Thereafter, the BSA loaded PLGA microspheres were suspended in 500 μL of PBS and placed at 37°C to obtain the drug release profile. At each time point, the microspheres were spun down and the supernatant was collected and equal volume of fresh PBS was added in. MicroBCA assay was utilized to obtain the amount of BSA in the supernatant at each time point. Three months later, the PLGA microspheres degraded completely and the supernatant was collected to obtain the amount of the remaining BCA. The drug loading efficiency was then calculated using the following equation:

$$Loading\ efficiency(\%) = \frac{Mass\ of\ BSA\ in\ the\ washing\ buffer + Mass\ of\ BSA\ released\ from\ the\ PLGA\ particles}{Total\ mass\ of\ BSA\ loaded} \times 100$$

Sciatic nerve crush and the administration of drug loaded PLGA microspheres. Female Sprague-Dawley rats (12 weeks, 250–300 g) were obtained from In Vivos Pte Ltd (Singapore) and divided into three groups, receiving blank PLGA microspheres (blank PLGA, $n=6$), sFRP2 loaded PLGA microspheres (PLGA-sFRP2, $n=6$), and WIF1 loaded PLGA microspheres (PLGA-WIF1, $n=6$). The schematic diagram of the surgical procedures is shown in Figure 1(b) the experimental descriptions can be found in Supplemental Table S1b-c. Briefly, rats were anesthetized and the right sciatic nerves were exposed and crushed using a surgical clip for three times (15 s each) with a 10 s interval. Thereafter, the PLGA microspheres containing 2 μg of drugs was reconstituted in 15 μL of PBS and injected distally to the crushed nerves using a microinjector (Nanoliter 2010 with MICRO4 Controller, WPI). In one batch of the rat, their sciatic nerves were crushed and the injured nerves were administered with drug-loaded PLGA microspheres immediately. These rats were kept for 1 week before being sacrificed. In another batch of rats, the sciatic nerves were crushed and the rats were kept for 1 week before the injured nerves were administered with drug-loaded PLGA microspheres. One week later, the rats were sacrificed and the sciatic nerves were retrieved.

The sciatic nerves of the third batch of rats were exposed and crushed the same as described above. At predetermined time points, the rats were sacrificed and the crushed nerves were retrieved (i.e. 0.5–12 h, 3, 7, 14, 21 days post injury).

Immunostaining

In vitro. Briefly, the fixed dissociated DRG neurons and DRG explants were washed with 1 × PBS for three times (5 min each). The cells were then permeabilized in 0.1% Triton X-100 in 1 × PBS for 15 min. Thereafter, the DRGs were incubated in non-specific blocking solution (5% goat serum) for 1 h at room temperature, followed by incubation with primary antibody, mouse-anti βIII-Tubulin (Tuj1, 1:1000) for overnight at 4°C. Following that, the DRG neurons were washed for three times with 1 × PBS and detected with Alexa Fluor 555 goat anti-mouse secondary antibody (1:500) at room temperature for 2 h followed by DAPI for 10 min. The cells were washed for three time with 1 × PBS and mounted with Fluoromount-G™.

For dissociated DRG neurons, at least 30 neurons per group were imaged from three glass coverslips. These stitched images have a very high resolution and can be zoomed in till individual neurites were discernible (Supplemental Figure S2). Brightfield images of these explants were not analyzed because it was not possible to differentiate the neurites from the background electrospun PCL microfibers. The total neurite length, as well as the length of the longest neurite were then quantified. For DRG explants, stitched images of at least three DRGs were taken per group. The average length of top 10 longest neurite as well as the longest neurite length were then quantified. All images were taken under Lecia fluorescent microscope (Leica DMi8) and all the quantifications were done using ImageJ software (NIH).

In vivo. The nerve guidance conduits and sciatic nerves were retrieved and post-fixed for overnight. Thereafter, the nerve conduits and the sciatic nerves were transferred to 15% sucrose for 24 h followed by 30% sucrose at 4°C until they were cryosectioned. Sciatic nerves as well as nerve conduits were sectioned into 20 μm thick horizontal sections and directly mounted onto the glass slides. For nerve guidance conduits and sciatic nerves, the frozen sections were washed three times with 1 × PBS. The samples were then permeabilized with 0.1% Triton X-100 in 1 × PBS for 15 min and blocked with 10% goat serum for 1 h before they were stained with primary antibody, chicken anti-NF200 (1:1000). Samples were subsequently washed three times with 1 × PBS and incubated with the following secondary antibody: Alexa Fluor 488 goat anti-Chicken secondary antibody (1:500) for 2 h followed by DAPI (1:1000) for 10 min at room temperature. The samples were washed for three time with 1 × PBS and mounted with Fluormount-G™.

Stitched images were taken under 10x magnification using a fluorescent microscope (Leica DMi8). Similarly, they have a very high resolution and can be zoomed in till individual neurites were discernible (Supplemental Figure S3). For nerve ingrowth measurements inside the nerve guidance conduits, three sections were quantified for each animal. The distance of nerve ingrowth was calculated from the proximal end of the nerve conduits. Besides that, the number of nerve fibers that passed through a certain distance was also quantified using ImageJ software (NIH).

Another set of frozen sections (i.e. crushed sciatic nerves as well as nerves that were crushed at different time points) were washed three time with 1 × PBS. The samples were permeabilized with 0.1% Triton X-100 in 1 × PBS for 15 min and blocked with 10% goat serum for 1 h before they were stained with primary antibody, rabbit anti-SCG10 (1:1000). Samples were subsequently washed three times with 1 × PBS and incubated with the following secondary antibody: Alexa Fluor 555 goat anti-Rabbit secondary antibody (1:500) for 2 h followed by DAPI (1:1000) for 10 min at room temperature. The samples were washed for three time with 1 × PBS and mounted with Fluormount-G™.

Both injured area and uninjured area were taken under confocal microscope (Zeiss LSM 800) at 20x magnification. Three sciatic nerve sections were imaged and the fluorescent pixel numbers of both injured and uninjured area were quantified using ImageJ software.

Statistical analysis. Outlier analysis was performed to exclude the outliers using GraphPad QuickCalcs software. One-way ANOVA and Tukey post hoc tests were

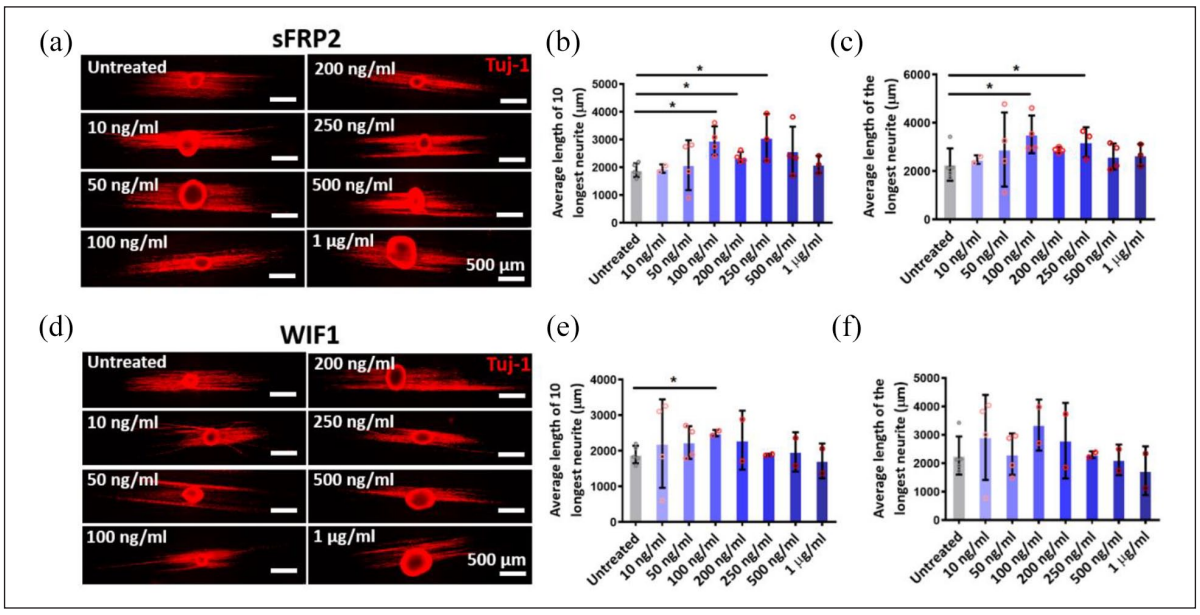

Figure 2. The treatment of WIF1 and sFRP2 promoted the neurite outgrowth of DRG explants. (a) Representative fluorescent images of Tuj-1 staining in DRG explants treated with sFRP2. (b and c) Quantification analysis of top 10 longest neurite length and the longest neurite length of DRG explants that are treated with sFRP2. (d) Representative fluorescent images of DRG explants treated with WIF1. (e and f) Quantification analysis of top 10 longest neurite length and the longest neurite length of DRG explants that are treated with WIF1. Data represented as mean ± SD. Shapiro-Wilk normality test followed by Kruskal-Wallis test and Mann-Whitney post hoc test.

used when data were normally distributed and had equal variances. For data that was not normally distributed or had unequal variances, the Kruskal–Wallis and Mann–Whitney *U* tests were used for comparison when more than two groups were included. For comparison between two groups, Student's *t*-test was used. Statistical analysis was done using SPSS software. All values were represented as mean ± SD.

Results

The treatment of WIF1 and sFRP2 promoted the neurite outgrowth of DRG explants

Figure 2(a) and (d) show the representative fluorescent images of Tuj1 stained DRG explants after the treatment of sFRP2 and WIF1, respectively. Quantification analysis of the average neurite length of top 10 longest neurite, as well as the longest neurite, indicated that treatment of sFRP2 (Figure 2(b) and (c)) could significantly promote the neurite outgrowth of DRG explants when the concentrations of the drug were around 100–250 ng/mL. Additionally, treatment of WIF1 also enhanced the neurite outgrowth of DRG explants when the concentration of WIF1 was around 100 ng/mL (Figure 2(e) and (f)). The same experiments were also carried out using dissociated DRG neurons with lower drug concentrations, as the dissociated DRG neuron were less tolerant than DRG explants. However, no significant enhancement in terms of neurite length was detected (Supplemental Figure S4).

The administration of WIF1 and sFRP2 exhibited little effects on promoting nerve regeneration after sciatic nerve transection

Figure 3(a) shows the SEM images of the nerve guidance conduit (cross-sectional view), where the lumen of the nerve conduit can be clearly seen. By quantifying the fiber diameter and the fiber angle, we observed that the encapsulation of sFRP2 and WIF1 did not alter the fiber diameter and alignment (Supplemental Figure S5a and b).

Figure 3(b) shows the representative fluorescent images of NF200 stained nerve guidance conduits 3 weeks after implantation. We observed that the regenerated nerve extended into the nerve guidance conduit from the proximal end and the aligned nerve guidance conduit could direct the regrowth of the nerve toward its distal end. Quantification of the distance of nerve ingrowth from the proximal end indicated that treatment of sFRP2 led to the longest length of nerve regeneration (7548 ± 663.5 µm) whereas the untreated samples (6504 ± 568.7 µm) and the WIF1 treated samples (6223 ± 837.7 µm) were relatively worse (Figure 3(c)). Besides that, the number of nerve fibers which passed through 2, 4, 6 mm from the proximal end was also calculated. Results show that there were significantly more nerve fibers that passed through the 6 mm

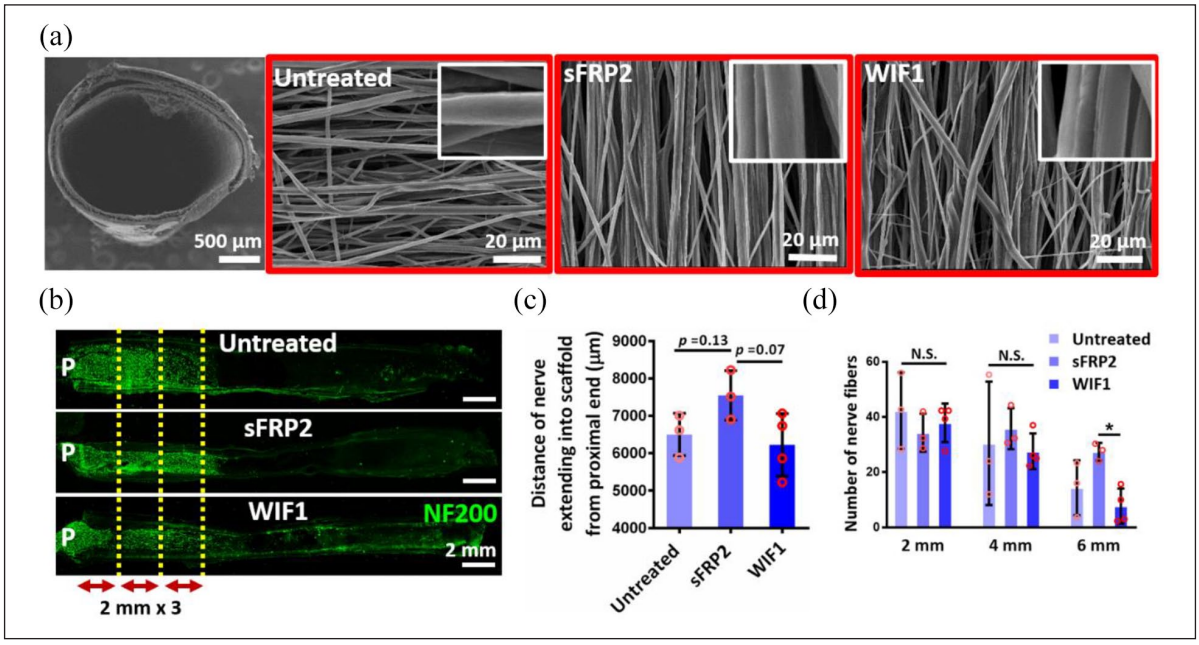

Figure 3. The administration of WIF1 and sFRP2 showed little effects on promoting nerve regeneration after sciatic nerve transection. (a) SEM images of the nerve guidance conduit (cross-sectional view) and the inner fiber morphology of plain fibers and fibers encapsulated with sFRP2 and WIF1. The inserts in the upper right corner are the enlarged images of individual fiber. (b) Representative fluorescent images of NF200 staining in untreated and sFRP2- and WIF1-treated rats. (c) Quantification analysis of the length of nerve regrowth calculated from the proximal end. (d) Quantification analysis of the number of nerve fibers that passed 2, 4, 6 mm distance, respectively. Data represented as mean ± SD, * $p < 0.05$, Shapiro-Wilk normality test followed by Kruskal-Wallis test and Mann-Whitney post hoc test.

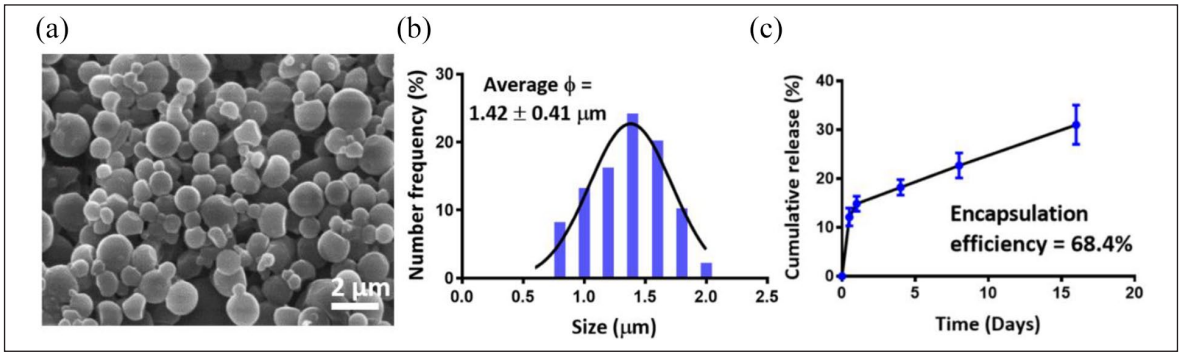

Figure 4. Characterizations of drug loaded PLGA microspheres. (a) SEM image of BSA-loaded PLGA microspheres. (b) Size distribution of the BSA-loaded PLGA microspheres. (c) The release profile of BSA from the PLGA microspheres.

distance from the proximal end in sFRP2-treated samples (Figure 3(d)).

Protein-based therapeutics were successfully loaded in the PLGA microspheres with a high loading efficiency

Figure 4(a) shows the SEM image of the BSA-loaded PLGA microspheres. The measurement of the particle size based on the SEM images showed that the average diameter was 1.42 ± 0.41 μm (Figure 4(b)). Following an initial rapid release within the first 24 h, PLGA microspheres provided a sustained release of BSA. About 30% of BSA was released from the PLGA microspheres at Day 16 and the drug loading efficiency was around 68.4% (Figure 4(c)). Considering that BSA has comparable molecular weight to sFRP2 and WIF1, we expect similar loading and release kinetics of these therapeutic proteins following PLGA microspheres encapsulation.

Mature axons did not reflect the effects of sFRP2 and WIF1 at Day 7 and Day 14 post crush injury

Figure 5(a) shows the representative stitched images of NF200 staining in blank PLGA-, PLGA-sFRP2-, and

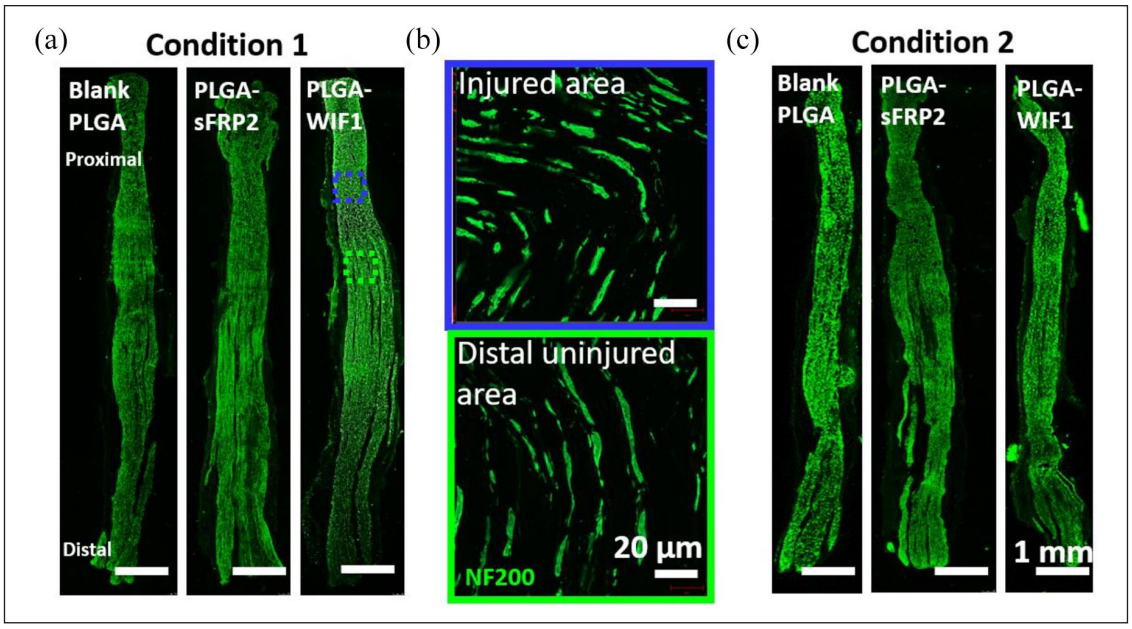

Figure 5. Mature axons do not reflect the effects of sFRP2 and WIF1 at Day 7 and Day 14 post injury. (a) Representative fluorescent images of NF200 staining in various groups under the condition of sciatic nerve crush and immediate treatment. (b) Confocal images of high magnification images of NF200 staining in the injured and distal uninjured area. (c) Representative fluorescent images of NF200 staining in various groups under the condition 2 (i.e. treatment was done 1 week post sciatic nerve crush).

PLGA-WIF1-treated rats under the condition of sciatic nerve crush and immediate treatment. The enlarged images of $NF200^{+}$ staining in Figure 5(b) showed that there was no clear difference in terms of mature axon regeneration between injured and distal uninjured regions. Figure 5(c) shows the representative stitched image of NF200 staining in blank PLGA-, PLGA-sFRP2-, and PLGA-WIF1-treated rats under the condition that sciatic nerve was crushed 1 week before the drug-loaded PLGA microspheres were administered. Under both conditions, the injured nerves were shown to regenerate well and there was no notable difference between injured and distal uninjured regions.

Under the condition that the treatments were given 1 week after sciatic nerve crush, the administration of WIF1 accelerated the regeneration of sciatic nerve

Next, we proceeded to evaluate the expression of SCG10, a marker which stains for regenerating axons[29,30] after sciatic nerve injuries. Besides that, the temporal expression of SCG10 at different time points (i.e. from 0.5 h to 21 days) were also uncovered (Supplemental Figure S6). As can be seen from Supplemental Figure S6a, SCG10 expression was completely absent in a normal uninjured sciatic nerve. On the contrary, the expression of SCG10 increased significantly in the injured region after sciatic nerve crush. Supplemental Figure S6b shows the enlarged images of SCG10 staining in both injured and distal uninjured regions (i.e. 1 mm below the injured region) at different time points. We revealed that there was almost no SCG10 expression in the distal uninjured area at 0.5 h after crush. As time went by, the expression of SCG10 in the distal uninjured area increased notably at day 3 and day 7 post crush (Supplemental Figure S6b). These findings suggest that, as the nerves regenerated, the expression of SCG10 also elongated along the regenerating nerves.

The ratio of fluorescent pixels of SCG10 expression in injury area versus distal uninjured area was then quantified and shown in Supplemental Figure S6c. Specifically, at 0.5 h post sciatic nerve crush, the expression of SCG10 in the injury region was quite high and the ratio of fluorescent pixels in the injured site versus distal uninjured area was around 32 (Supplemental Figure S6c). As the nerves regenerated, the expression of SCG10 increased in the distal uninjured region and hence the ratio of SCG10 fluorescent pixels in injured versus distal uninjured area started to decrease. We observed that for a normal uninjured nerve, there is no expression of SCG10, so the ratio of SCG10 fluorescent pixels in injured versus distal uninjured area tends to be 1. At 21 days post injury, the expression of SCG10 in the injured area versus distal uninjured nerve tends to be equal and hence the ratio of SCG10 fluorescent pixels is close to 1, suggesting that when an injured nerve completes its regeneration, the expression of SCG10 tends to return to normalcy in the regenerated regions. Therefore, the low expression of SCG10 indicated an accomplished nerve regeneration at Day 7 after sciatic nerve crush injury onwards.

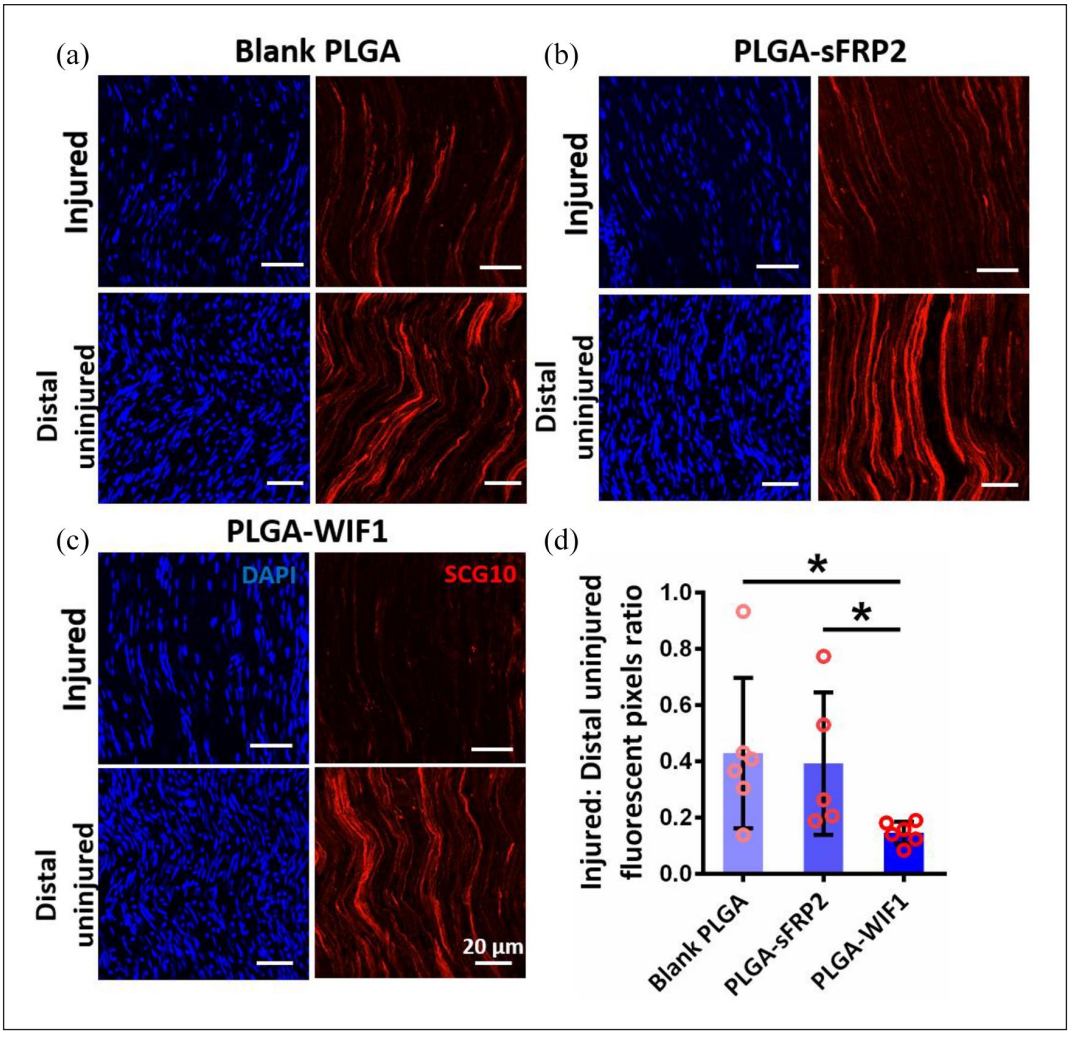

Figure 6. Under the condition that the treatments were given 1 week after sciatic nerve crush, the administration of WIF1 accelerated the regeneration of sciatic nerve. (a–c) Representative fluorescent images of SCG10 staining in both injured and distal uninjured area in in blank PLGA-, PLGA-sFRP2-, and PLGA-WIF1-treated samples. (d) Quantification analysis of the ratio of fluorescent pixel between injured and distal uninjured area in different treatment groups. Data represented as mean ± SD, $*p < 0.05$, Shapiro-Wilk normality test followed by Kruskal-Wallis test and Mann-Whitney post hoc test.

Figure 6(a) to (c) show the representative fluorescent images of SCG10 staining in both injured versus distal uninjured region in blank PLGA-, PLGA-sFRP2-, and PLGA-WIF1-treated samples. By quantifying the ratio of SCG10 fluorescent pixels in the injured versus distal uninjured area, we observed that in PLGA-WIF1-treated samples, the ratio was significantly lower as compared to untreated and PLGA-sFRP2-treated sciatic nerves (Figure 6(d)). This suggests that nerve regeneration in the injured region was faster in PLGA-WIF1-treated samples, as compared to PLGA-sFRP2-treated samples. Therefore, the treatment of WIF1 accelerated the regeneration of sciatic nerve after crush injury. On the other hand, under the condition that the treatment was given immediately after sciatic nerve crush, Wnt inhibitors did not promote the regeneration of the injured axons (Supplemental Figure S7).

Discussion

Injuries to the PNS are not fatal.[31] However, post injury symptoms, such as sensory and motor deficits[32] as well as neuropathic pain,[33] strongly impair patients' quality of life.[34] Therefore, exploring potential therapeutics that promote the regeneration of the injured sciatic nerve is of great necessity. Growth factors have been widely utilized to stimulate the regrowth of injured sciatic nerves.[35–37] However, growth factors-based treatment may be less effective in cases where the expression of their receptors on the neuronal surface is low.[38] While many studies looked into enhancing/overexpressing growth promoting factors to improve axon regeneration,[39–41] it is also essential to look at the other side of the coin, which is to block/downregulate the growth inhibitory factors that hinder

nerve regeneration. Therefore, in this work, we focused on looking at pathway inhibition/silencing approach by which the nerve growth inhibitors can be downregulated, and investigated the potential of this approach in enhancing nerve regeneration following sciatic nerve injuries.

Here, two Wnt signaling inhibitors, WIF1 and sFRP2, were utilized to block the repulsive Wnt signaling pathway. Specifically, WIF1 is a secreted Wnt inhibitor, which exerts its inhibitory effect on Wnt signaling by binding directly to Wnt ligands and preventing the Wnt ligands from binding to their receptors.[42] sFRP2 is a secreted frizzled-related protein, which suppresses the Wnt/β-catenin signaling pathway.[43] Their effects on neurite outgrowth were firstly evaluated in vitro using DRG neurons. Treatment of sFRP2 (250 ng/mL) and WIF1 (100 ng/mL) induced significantly longer neurite extension (~3500–3300 μm respectively, Figure 2), which was about 1.47- to 1.56-fold enhancement as compared to untreated DRG neurons. Growth factors and other small molecules were also commonly used to promote neurite outgrowth in neurons. For instance, the pain reliever Ibuprofen, which inhibits the activation of RhoA (Ras homolog gene family, member A GTPase where most of the glial growth inhibiting factors converge), promoted neurite outgrowth in human model neurons by about 1.4-fold.[44] Besides that, anti-inflammatory cytokine, interleukin-10 (IL-10), which provides neuroprotection in cerebral ischemia was shown to enhance the neurite outgrowth by about 1.34-fold in cultured cortical neurons.[45] Stem cell factor (SCF) and granulocyte colony-stimulating factor (G-CSF), which regulate bone marrow stem cell proliferation and differentiation, were reported to promote neurite outgrowth from cortical neurons by about 1.4-fold when they were used as a cocktail.[46] Comparing these findings with ours, Wnt signaling inhibitors, sFRP2 and WIF1, were quite prominent in promoting neurite outgrowth in DRG neurons.

Due to the short lifespan of protein-based therapeutics, biomaterials-based drug delivery approaches were adopted to prolong the availability of the drugs.[13–19] Engineered nerve guidance conduits and/or polymeric microspheres have been frequently applied in PNS applications.[47–50] Specifically, by encapsulating the therapeutics of interest into electrospun nerve conduits, a sustained availability of bioactive drugs can be achieved.[13,14] Besides that, the topographical cues provided by aligned electrospun fibers within the nerve guidance conduits can further direct and enhance nerve regeneration (Figure 3(a) and Supplemental Figure S3). Additionally, we further fashioned the exterior with a dense and hydrophobic PCL film to prevent surrounding cells such as fibroblast from infiltrating. On the other hand, microspheres fabricated by polymers, such as PLGA, were applied as drug loading vehicles due to their biocompatibility and high drug loading efficiency.[51,52] PLGA (PLA/PGA 50:50) was utilized for the fabrication of drug-loaded microspheres due to its faster degradation rate than PLGA 65:35.[53] The fast degradation rate of PLGA microspheres also facilitated a sustained release of the therapeutics (Figure 4), which is suitable for long term studies. The loading efficiency (~68.4%) was also comparable with a similar study where bone morphogenetic protein 2 (BMP-2, similar molecular weight with Wnt inhibitors) was encapsulated in PLGA microspheres.[54]

PLGA has been widely used to encapsulate drugs,[55–58] peptides,[59–61] proteins[62–66] as well nucleic acids[67,68] due to their biocompatibility and biodegradability. In studies which specifically utilized PLGA microspheres for protein delivery (e.g. VEGF, FGF),[62,64] there were no issues with the stability of the encapsulated biologics and the bioactivity of the proteins was fully preserved. Some of these studies also obtained a similar release profile which included an initial burst release followed by a sustained release over time.[56,57,62,67] Subsequently, the released materials, some despite being pH sensitive, were able to induce biological effects, demonstrating the retention of their bioactivity throughout the encapsulation and release process. As the drugs utilized in our study were proteinaceous in nature, it is therefore very likely that they also remained stable and retained their bioactivity throughout the fabrication and release process. This was further supported by the significant biological outcomes observed in our experiments (Figure 6).

Sciatic nerve transection and nerve conduit implantation is a widely used injury model to evaluate the efficacy of a therapeutic with the synergistic effects from both the biochemical signaling and topographical guidance. It has been reported previously that neurotrophic factors can enhance nerve regeneration across short distances (up to 10 mm).[69,70] This distance is achievable for axons to regenerate through nerve guidance conduits in the absence of exogenous trophic support.[71] However, as the nerve gaps are often longer in clinical practice, a 15-mm critical nerve defect gap was created here instead of the usual 10-mm gap so as to induce a severe injury model for a more practical evaluation of nerve regrowth. The two Wnt signaling inhibitors, sFRP2 and WIF1, were encapsulated in electrospun fiber conduits and implanted to the injured sciatic nerve. Both of the drugs can competitively bind to Wnt ligands, leading to the inhibition of Wnt binding to Ryk.[4] The regrowth of neurofilament into the nerve conduit in sFRP2-treated rats was up to ~7500 μm, which is even longer than axonal-promoting microRNAs (i.e. miR-132/miR-222/miR-431)-treated samples (~6200 μm) using the same injury model at the same time point.[26] Additionally, in the work done by Kolar et al., when human dental mesenchymal stem cells (D-MSCs), demonstrated to secrete BDNF, GDNF, NGF, and VEGFA, were encapsulated into the nerve conduit for rat sciatic nerve implantation, the rate of neurofilament regrowth was about 2.5 mm/week,[72] which was comparable as what we obtained here using Wnt signaling inhibitors (2.5 mm/week). In this work,

there is a trend that treatment of sFRP2 could enhance nerve regeneration in contrast to the untreated samples (1000 μm longer than untreated samples, $p = 0.13$, Figure 3(b) and (c)) but without statistical significance. One possible reason is that in the sciatic nerve transection model, the non-canonical Wnt receptor Ryk might not have been sufficiently upregulated for the inhibitors to take effect. Alternatively, it could be that the axon-promoting canonical Wnt signaling[8,9] was activated instead. More work needs to be conducted in future to reveal the signaling pathway changes after sciatic nerve transection injury.

As sciatic nerve crush injury is another common peripheral nerve injury in the clinic, it was also used in this work to evaluate nerve regeneration after the inhibition of the Wnt signaling pathway. After sciatic nerve crush, the distal stump of the injured nerve undergoes Wallerian degeneration,[73] which is indicated by tissue degeneration and myelin debris clearance.[74,75] Therefore, the signaling pathways after crush injury also undergo drastic changes. Specifically, the repulsive Wnt-Ryk signaling pathway was upregulated 1 week after sciatic nerve crush and led to nerve retraction.[4] In order to find out if the inhibition of the repulsive Wnt-Ryk signaling for nerve regeneration is time-dependent, the Wnt inhibitors were administered at two different time points (i.e. immediately after crush and 1 week after crush).

NF200 was firstly utilized to evaluate the nerve regrowth. However, NF200 staining was unable to differentiate the existing uninjured axons and the regenerating axons (Figure 5). As such, we used SCG10, also known as stathmin 2 (STMN2), as axonal SCG10 is dynamically regulated upon nerve injury and is shown to be a selective marker for regenerating sensory axons.[30]

As time goes by, the expression of SCG10 propagated along the regenerating nerves (Supplemental Figure S6a–c), which is in good agreement with the study by Shin et al.[30] In their work, the expression of SCG10 increased consistently over time post injury.[30] Another similar study where growth associated protein 43 (GAP43) was utilized for the evaluation of nerve regeneration after sciatic nerve crush, Dubovy et al. demonstrated that after sciatic nerve compression, the expression of GAP43 increased consistently from Day 1 to Day 7 in the associated DRG neurons. However, the expression of GAP43 decreased from Day 7 to Day 14, indicating a dynamic role of GAP43 expression after sciatic nerve compression.[29] Linking back to our findings where the expression of SCG10 in the injured area decreased significantly at the evaluation time point, it is reasonable to conclude that when the injured axons completed their regeneration, the expression of SCG10 reverted to normalcy and is similar to an uninjured normal sciatic nerve (Supplemental Figure S6). Hence, a low expression of SCG10 at the injured region suggested that the axons there might have regenerated from Day 7 onwards.

In the current work, we demonstrated that when WIF1 was administered 1 week after sciatic nerve crush, the expression of SCG10 in the injured region decreased faster (Figure 6(a)–(c)). The ratio of SCG10 expression between the injured and distal uninjured region was significantly lower as compared to the blank-PLGA- and PLGA-sFRP2-treated samples (Figure 6(d)), indicating that the treatment of WIF1 could accelerate axonal regeneration after crush injury. One possible reason for this is WIF1 shares sequence homology with the Wnt-binding domain of Ryk[76] and hence the inhibition of the repulsive Wnt-Ryk signaling is more specific as compared to sFRP2 which targets more on Wnt-Frizzled binding. However, when the drugs were administered immediately after sciatic nerve crush, the effects of WIF1 and sFRP2 were not apparent. An important implication of this work is the utilization of SCG10 staining to assess the regeneration of the injured sciatic nerves, besides the conventional NF200 staining, which is widely utilized but provide less insightful results. One may miss out important conclusions by picking the wrong marker. Besides that, future studies should include electron microscopy images to further enhance the credibility of the findings. Another important implication of this finding is that Wnt inhibitors only exert positive effects on nerve regeneration when non-canonical Ryk is significant upregulated in the injured area. Within the PNS, the expression of Ryk was upregulated significantly in the sciatic nerve 1 week after conditioning lesion.[4] The addition of Wnt inhibitors at this time is the therapeutic window for the Wnt inhibitors to take effect.

Conclusions

In this work, sciatic nerve transection and sciatic nerve crush models were applied to thoroughly evaluate the effects of Wnt inhibitors, WIF1 and sFRP2, in promoting nerve regeneration. Our results demonstrated that WIF1, could promote nerve regeneration after sciatic nerve crush injury. More importantly, we revealed the therapeutic window of using Wnt inhibitors to enhance nerve regeneration, which is under the circumstance that non-canonical Ryk is significantly upregulated.

Acknowledgements

Na Zhang would like to acknowledge the support of Nanyang Technological University (NTU) by providing NTU Research Scholarship to carry out these research works. Prof. Ahmet Hoke from John Hopkins University is acknowledged for the valuable discussions and suggestions.

Author contributions

S. Y. C. conceptualized the study and designed the project. D. A. M. provided valuable suggestions and discussions on the experiments performed. N. Z. performed the in vitro cell culture. J. S. C. fabricated the electrospun nerve conduits. C. W. and C. X. fabricated the PLGA microspheres. N. Z. and J. L. performed the characterizations of electrospun nerve conduits and PLGA

microspheres, in vivo animal experiments, data analysis, and figures drawing. N. Z. and S. Y. C. drafted the manuscript. S. Y. C and D. A. M. obtained the funding support for this project.

Declaration of conflicting interests

The author(s) declared no potential conflicts of interest with respect to the research, authorship, and/or publication of this article.

Funding

The author(s) disclosed receipt of the following financial support for the research, authorship, and/or publication of this article: Financial support was received from SingHealth-NTU research collaborative grant (SHS-NTU/038/2016) and MOE AcRF Tier 1 grant (RG37/20).

ORCID iD

Sing Yian Chew https://orcid.org/0000-0002-6084-5967

Supplemental material

Supplemental material for this article is available online.

References

1. Zhang Y, Zhan Y, Han N, et al. Analysis of temporal expression profiles after sciatic nerve injury by bioinformatic method. *Sci Rep* 2017; 7(1): 9818.
2. Qian T, Fan C, Liu Q, et al. Systemic functional enrichment and ceRNA network identification following peripheral nerve injury. *Mol Brain* 2018; 11(1): 73.
3. Liu Y, Wang X, Lu CC, et al. Repulsive Wnt signaling inhibits axon regeneration after CNS injury. *J Neurosci* 2008; 28(33): 8376–8382.
4. Hollis E 2nd and Zou Y. Reinduced Wnt signaling limits regenerative potential of sensory axons in the spinal cord following conditioning lesion. *Proc Natl Acad Sci USA* 2012; 109(36): 14663–14668.
5. Zou Y. Wnt signaling in axon guidance. *Trends Neurosci* 2004; 27(9): 528–532.
6. Onishi K, Hollis E and Zou Y. Axon guidance and injury-lessons from Wnts and Wnt Signaling. *Curr Opin Neurobiol* 2014; 27: 232–240.
7. Schmitt AM, Shi J, Wolf AM, et al. Wnt-Ryk signalling mediates medial-lateral retinotectal topographic mapping. *Nature* 2006; 439(7072): 31–37.
8. Alavian KN, Li H, Collis L, et al. Bcl-xL regulates metabolic efficiency of neurons through interaction with the mitochondrial F1FO ATP synthase. *Nat Cell Biol* 2011; 13(10): 1224–1233.
9. Han Z, Ge X, Tan J, et al. Establishment of lipofection protocol for efficient miR-21 transfection into cortical neurons in vitro. *DNA Cell Biol* 2015; 34(12): 703–709.
10. Miyashita T, Koda M, Kitajo K, et al. Wnt-Ryk signaling mediates axon growth inhibition and limits functional recovery after spinal cord Injury. *J Neurotrauma* 2009; 26(7): 955–964.
11. Yam PT and Charron F. Signaling mechanisms of non-conventional axon guidance cues: the Shh, BMP and Wnt morphogens. *Curr Opin Neurobiol* 2013; 23: 965–973.
12. Salinas PC. Wnt signaling in the vertebrate central nervous system: from axon guidance to synaptic function. *Cold Spring Harb Perspect Biol* 2012; 4(2): DOI: 10.1101/cshperspect.a008003 : 1–14.
13. Milbreta U, Lin J, Pinese C, et al. Scaffold-mediated sustained, non-viral delivery of miR-219/miR-338 promotes CNS remyelination. *Mol Ther* 2019; 27(2): 411–423.
14. Zhang N, Milbreta U, Chin JS, et al. Biomimicking fiber scaffold as an effective in vitro and in vivo MicroRNA screening platform for directing tissue regeneration. *Adv Sci* 2019; 6(9): 1800808.
15. Diao HJ, Low WC, Milbreta U, et al. Nanofiber-mediated microRNA delivery to enhance differentiation and maturation of oligodendroglial precursor cells. *J Control Release* 2015; 208: 85–92.
16. Pinese C, Lin J, Milbreta U, et al. Sustained delivery of siRNA/mesoporous silica nanoparticle complexes from nanofiber scaffolds for long-term gene silencing. *Acta Biomater* 2018; 76: 164–177.
17. Low WC, Rujitanaroj P-O, Lee D-K, et al. Nanofibrous scaffold-mediated REST knockdown to enhance neuronal differentiation of stem cells. *Biomaterials* 2013; 34(14): 3581–3590.
18. Jiang X, Cao HQ, Shi LY, et al. Nanofiber topography and sustained biochemical signaling enhance human mesenchymal stem cell neural commitment. *Acta Biomater* 2012; 8(3): 1290–1302.
19. Low WC, Rujitanaroj P-O, Wang F, et al. Nanofiber-mediated release of retinoic acid and brain-derived neurotrophic factor for enhanced neuronal differentiation of neural progenitor cells. *Drug Deliv Transl Res* 2015; 5(2): 89–100.
20. Guo W, Quan P, Fang L, et al. Sustained release donepezil loaded PLGA microspheres for injection: preparation, in vitro and in vivo study. *Asian J Pharm Sci* 2015; 10(5): 405–414.
21. Zhang Z, Wang X, Li B, et al. Paclitaxel-loaded PLGA microspheres with a novel morphology to facilitate drug delivery and antitumor efficiency. *RSC Adv* 2018; 8(6): 3274–3285.
22. Bao W, Zhou J, Luo J, et al. PLGA microspheres with high drug loading and high encapsulation efficiency prepared by a novel solvent evaporation technique. *J Microencapsul* 2006; 23(5): 471–479.
23. Yi S, Zhang H, Gong L, et al. Deep sequencing and bioinformatic analysis of lesioned sciatic nerves after crush injury. *PLoS One* 2015; 10(12): e0143491.
24. Li S, Liu Q, Wang Y, et al. Differential gene expression profiling and biological process analysis in proximal nerve segments after sciatic nerve transection. *PLoS One* 2013; 8(2): e57000.
25. Gong L, Wang D, Zhang L, et al. Genetic changes in rat proximal nerve stumps after sciatic nerve transection. *Ann Transl Med* 2019; 7(23): 763–763.
26. Zhang N, Lin J, Chin JS, et al. A laser microdissection-based axotomy model incorporating the use of biomimicking fiber scaffolds reveals that microRNAs promote axon regeneration over long injury distances. *Biomater Sci* 2020; 8: 6286–6300.
27. Kele J, Andersson ER, Villaescusa JC, et al. SFRP1 and SFRP2 dose-dependently regulate midbrain dopamine neu-

ron development in vivo and in embryonic stem cells. *Stem Cells* 2012; 30(5): 865–875.
28. Hu J, Dong A, Fernandez-Ruiz V, et al. Blockade of Wnt signaling inhibits angiogenesis and tumor growth in hepatocellular carcinoma. *Cancer Res* 2009; 69(17): 6951–6959.
29. Dubový P, Klusáková I, Hradilová-Svíženská I, et al. A conditioning sciatic nerve lesion triggers a pro-Regenerative state in primary sensory neurons also of dorsal root ganglia Non-Associated with the damaged nerve. *Front Cell Neurosci* 2019; 13: 11.
30. Shin JE, Geisler S and DiAntonio A. Dynamic regulation of SCG10 in regenerating axons after injury. *Exp Neurol* 2014; 252: 1–11.
31. Menorca RMG, Fussell TS and Elfar JC. Peripheral nerve trauma: mechanisms of injury and recovery. *Hand Clin* 2013; 29(3): 317–330.
32. Hussain G, Wang J, Rasul A, et al. Current status of therapeutic approaches against peripheral nerve injuries: a detailed story from injury to recovery. *Int J Biol Sci* 2020; 16: 116–134.
33. Meacham K, Shepherd A, Mohapatra DP, et al. Neuropathic pain: central vs. peripheral mechanisms. *Curr Pain Headache Rep* 2017; 21: 28.
34. Grinsell D and Keating CP. Peripheral Nerve Reconstruction after injury: a review of clinical and experimental therapies. *Biomed Res Int* 2014; 2014: 1–13.
35. Ma S, Peng C, Wu S, et al. Sciatic nerve regeneration using a nerve growth factor-containing fibrin glue membrane. *Neural Regen Res* 2013; 8(36): 3416–3422.
36. Li R, Li D-H, Zhang H-Y, et al. Growth factors-based therapeutic strategies and their underlying signaling mechanisms for peripheral nerve regeneration. *Acta Pharmacol Sin* 2020; 41: 1289–1300.
37. Zhang R, Zhang Y and Yi S. Identification of critical growth factors for peripheral nerve regeneration. *RSC Adv* 2019; 9(19): 10760–10765.
38. Singh B, Singh V, Krishnan A, et al. Regeneration of diabetic axons is enhanced by selective knockdown of the PTEN gene. *Brain* 2014; 137(4): 1051–1067.
39. Lee AC, Yu VM, Lowe JB 3rd, et al. Controlled release of nerve growth factor enhances sciatic nerve regeneration. *Exp Neurol* 2003; 184(1): 295–303.
40. Fang Z, Ge X, Chen X, et al. Enhancement of sciatic nerve regeneration with dual delivery of vascular endothelial growth factor and nerve growth factor genes. *J Nanobiotechnol* 2020; 18(1): 46.
41. Zhang N, Chin JS and Chew SY. Localised Non-Viral delivery of nucleic acids for nerve regeneration in injured nervous systems. *Exp Neurol* 2019; 319: 112820.
42. Ng RC, Matsumaru D, Ho AS, et al. Dysregulation of Wnt inhibitory factor 1 (Wif1) expression resulted in aberrant Wnt-β-catenin signaling and cell death of the cloaca endoderm, and anorectal malformations. *Cell Death Differ* 2014; 21(6): 978–989.
43. Lee JL, Chang CJ, Chueh LL, et al. Secreted frizzled related protein 2 (sFRP2) decreases susceptibility to UV-induced apoptosis in primary culture of canine mammary gland tumors by NF-kappaB activation or JNK suppression. *Breast Cancer Res Treat* 2006; 100(1): 49–58.
44. Roloff F, Scheiblich H, Dewitz C, et al. Enhanced neurite outgrowth of human model (NT2) neurons by small-molecule inhibitors of Rho/ROCK signaling. *PLoS One* 2015; 10(2): e0118536.
45. Chen H, Lin W, Zhang Y, et al. IL-10 promotes neurite outgrowth and synapse formation in cultured cortical neurons after the oxygen-glucose deprivation via JAK1/STAT3 pathway. *Sci Rep* 2016; 6: 30459.
46. Su Y, Cui L, Piao C, et al. The effects of hematopoietic growth factors on neurite outgrowth. *PLoS One* 2013; 8(10): e75562.
47. Chew SY, Mi R, Hoke A, et al. Aligned protein-polymer composite fibers enhance nerve regeneration: a potential tissue-engineering platform. *Adv Funct Mater* 2007; 17(8): 1288–1296.
48. Jiang X, Mi R, Hoke A, et al. Nanofibrous nerve conduit-enhanced peripheral nerve regeneration. *J Regen Med Tissue Eng* 2014; 8(5): 377–385.
49. Xu X, Yu H, Gao S, et al. Polyphosphoester microspheres for sustained release of biologically active nerve growth factor. *Biomaterials* 2002; 23(17): 3765–3772.
50. de Boer R, Knight AM, Spinner RJ, et al. In vitro and in vivo release of nerve growth factor from biodegradable poly-lactic-co-glycolic-acid microspheres. *J Biomed Mater Res A* 2010; 95(4): 1067–1073.
51. Han FY, Thurecht KJ, Whittaker AK, et al. Bioerodable PLGA-based microparticles for producing sustained-release drug formulations and strategies for improving drug loading. *Front Pharmacol* 2016; 7: 185.
52. Musumeci T, Ventura CA, Giannone I, et al. PLA/PLGA nanoparticles for sustained release of docetaxel. *Int J Pharm* 2006; 325(1–2): 172–179.
53. Park TG. Degradation of poly(lactic-co-glycolic acid) microspheres: effect of copolymer composition. *Biomaterials* 1995; 16(15): 1123–1130.
54. Kirby GTS, White LJ, Rahman CV, et al. PLGA-based microparticles for the sustained release of BMP-2. *Eur Cell Mater* 2011; 22: 24.
55. Feng S, Nie L, Zou P, et al. Drug-loaded PLGA-mpeg microparticles as treatment for atopic dermatitis-like skin lesions in BALB/c mice model. *J Microencapsul* 2015; 32(2): 201–209.
56. Obayemi JD, Danyuo Y, Dozie-Nwachukwu S, et al. PLGA-based microparticles loaded with bacterial-synthesized prodigiosin for anticancer drug release: Effects of Particle Size on drug release kinetics and cell viability. *Mater Sci Eng C* 2016; 66: 51–65.
57. Regnier-Delplace C, Thillaye du Boullay O, Siepmann F, et al. PLGA microparticles with zero-order release of the labile anti-Parkinson drug apomorphine. *Int J Pharm* 2013; 443(1–2): 68–79.
58. SreeHarsha N, Venugopala KN, Nair AB, et al. An efficient, lung-targeted, drug-delivery system to treat asthma via microparticles. *Drug Des Dev Ther* 2019; 13: 4389–4403.
59. Li Y, Na R, Wang X, et al. Fabrication of antimicrobial peptide-loaded PLGA/chitosan composite microspheres for long-acting bacterial resistance. *Molecules* 2017; 22(10): 1–12.
60. Herrmann VL, Wieland DE, Legler DF, et al. The STEAP1262-270 peptide encapsulated into PLGA microspheres elicits strong cytotoxic T cell immunity in HLA-A*0201 transgenic mice: a new approach to immunotherapy against prostate carcinoma. *Prostate* 2016; 76(5): 456–468.

61. Choi YH, Heo SC, Kwon YW, et al. Injectable PLGA microspheres encapsulating WKYMVM peptide for neovascularization. *Acta Biomater* 2015; 25: 76–85.
62. Simón-Yarza T, Formiga FR, Tamayo E, et al. PEGylated-PLGA microparticles containing VEGF for long term drug delivery. *Int J Pharm* 2013; 440(1): 13–18.
63. Yu Z, Huang L, Wen R, et al. Preparation and in vivo pharmacokinetics of rhGH-Loaded PLGA microspheres. *Pharm Dev Technol* 2019; 24(4): 395–401.
64. Kim DH, Huegel J, Taylor BL, et al. Biocompatibility and bioactivity of an FGF-loaded microsphere-based bilayer delivery system. *Acta Biomater* 2020; 111: 341–348.
65. Wang X, Qi F, Xing H, et al. Uniform-sized insulin-loaded PLGA microspheres for improved early-stage peri-implant bone regeneration. *Drug Deliv* 2019; 26(1): 1178–1190.
66. Cleland JL, Mac A, Boyd B, et al. The stability of recombinant human growth hormone in poly(lactic-co-glycolic acid) (PLGA) microspheres. *Pharm Res* 1997; 14(4): 420–425.
67. Présumey J, Salzano G, Courties G, et al. PLGA microspheres encapsulating siRNA anti-TNFalpha: efficient RNAi-mediated treatment of arthritic joints. *Eur J Pharm Biopharm* 2012; 82(3): 457–464.
68. Lunsford L, McKeever U, Eckstein V, et al. Tissue distribution and persistence in mice of plasmid DNA encapsulated in a PLGA-based microsphere delivery vehicle. *J Drug Target* 2000; 8(1): 39–50.
69. Terenghi G. Peripheral nerve regeneration and neurotrophic factors. *J Anat* 1999; 194 (Pt 1): 1–14.
70. Frostick SP, Yin Q and Kemp GJ. Schwann cells, neurotrophic factors, and peripheral nerve regeneration. *Microsurgery* 1998; 18(7): 397–405.
71. Jenq CB and Coggeshall RE. Nerve regeneration through holey silicone tubes. *Brain Res* 1985; 361(1–2): 233–241.
72. Kolar MK, Itte VN, Kingham PJ, et al. The neurotrophic effects of different human dental mesenchymal stem cells. *Sci Rep* 2017; 7(1): 12605.
73. Rotshenker S. Wallerian degeneration: the innate-immune response to traumatic nerve injury. *J Neuroinflammation* 2011; 8: 109.
74. Dubový P. Wallerian degeneration and peripheral nerve conditions for both axonal regeneration and neuropathic pain induction. *Ann Anat* 2011; 193(4): 267–275.
75. Gaudet AD, Popovich PG and Ramer MS. Wallerian degeneration: gaining perspective on inflammatory events after peripheral nerve injury. *J Neuroinflammation* 2011; 8: 110.
76. Macheda ML, Sun WW, Kugathasan K, et al. The Wnt receptor Ryk plays a role in mammalian planar cell polarity signaling. *J Biol Chem* 2012; 287(35): 29312–29323.